AFRL-RX-WP-JA-2016-0259

ADVANCES IN THE DEVELOPMENT OF PROCESSING MICROSTRUCTURE RELATIONS FOR TITANIUM ALLOYS (POSTPRINT)

S.L. Semiatin and A.L. Pilchak

AFRL/RX

23 JUNE 2015
Interim Report

(STINFO COPY)

AIR FORCE RESEARCH LABORATORY
MATERIALS AND MANUFACTURING DIRECTORATE
WRIGHT-PATTERSON AIR FORCE BASE, OH 45433-7750
AIR FORCE MATERIEL COMMAND
UNITED STATES AIR FORCE

REPORT DOCUMENTATION PAGE

Form Approved
OMB No. 0704-0188

1. REPORT DATE *(DD-MM-YY)*	2. REPORT TYPE	3. DATES COVERED *(From - To)*
23 June 2015	Interim	19 March 2014 – 23 May 2015

4. TITLE AND SUBTITLE
ADVANCES IN THE DEVELOPMENT OF PROCESSING MICROSTRUCTURE RELATIONS FOR TITANIUM ALLOYS (POSTPRINT)

5a. CONTRACT NUMBER
IN-HOUSE

5b. GRANT NUMBER

5c. PROGRAM ELEMENT NUMBER

6. AUTHOR(S)
S.L. Semiatin and A.L. Pilchak -
AFRL/RX

5d. PROJECT NUMBER

5e. TASK NUMBER

5f. WORK UNIT NUMBER
X0W6

7. PERFORMING ORGANIZATION NAME(S) AND ADDRESS(ES)
AFRL/RX
Wright-Patterson AFB, OH
45433-7750

8. PERFORMING ORGANIZATION REPORT NUMBER

9. SPONSORING/MONITORING AGENCY NAME(S) AND ADDRESS(ES)
Air Force Research Laboratory
Materials and Manufacturing Directorate
Wright-Patterson Air Force Base, OH 45433-7750
Air Force Materiel Command
United States Air Force

10. SPONSORING/MONITORING AGENCY ACRONYM(S)
AFRL/RXCM

11. SPONSORING/MONITORING AGENCY REPORT NUMBER(S)
AFRL-RX-WP-JA-2016-0259

12. DISTRIBUTION/AVAILABILITY STATEMENT
Distribution Statement A. Approved for public release: distribution unlimited.

13. SUPPLEMENTARY NOTES
PA Case Number: 88ABW-2015-3157; Clearance Date: 23 June 2015. This document contains color. Journal article published in Proceedings of the 13th World Conference on Titanium, Ch. 29, 6 May 2016.
The final publication is available at DOI: 10.1002/9781119296126.ch29

14. ABSTRACT *(Maximum 200 words)*
Advances in the fundamental understanding of microstructure evolution and plastic flow during primary and secondary processing of titanium alloys are summarized. Examples focus on the recrystallization of the beta phase and spheroidization of alpha lamellae during the breakdown of α/β titanium alloys, challenges in the rolling of foil of α/β and gamma-TiAl alloys, and the effect of microstructure and composition on the superplastic flow behavior of α/β titanium alloys. Particular attention is given to models describing the refinement (or coarsening) of microstructural scale and non-uniformities that may impact forming response during operations such as rolling of sheet and superplastic forming. Current understanding of the persistence of microstructural anomalies such as microtextured regions (aka macrozones) is also described. Finally, recent developments in the characterization of such features via microscopy and ultrasonics are discussed.

15. SUBJECT TERMS
Alpha/beta titanium alloys, recrystallization, spheroidization, foil rolling, low-temperature superplasticity, texture

16. SECURITY CLASSIFICATION OF:			17. LIMITATION OF ABSTRACT:	18. NUMBER OF PAGES	19a. NAME OF RESPONSIBLE PERSON (Monitor)
a. REPORT	b. ABSTRACT	c. THIS PAGE			Bill Song
Unclassified	Unclassified	Unclassified	SAR	14	19b. TELEPHONE NUMBER *(Include Area Code)* (937) 255-1351

Proceedings of the 13th World Conference on Titanium
Edited by: Vasisht Venkatesh, Adam L. Pilchak, John E. Allison, Sreeramamurthy Ankem, Rodney Boyer, Julie Christodoulou, Hamish L. Fraser, M. Ashraf Imam, Yoji Kosaka, Henry J. Rack, Amit Chatterjee, and Andy Woodfield
TMS (The Minerals, Metals & Materials Society), 2016

ADVANCES IN THE DEVELOPMENT OF PROCESSING-MICROSTRUCTURE RELATIONS FOR TITANIUM ALLOYS

S.L. Semiatin and A.L. Pilchak
Air Force Research Laboratory, AFRL/RXCM,
Wright-Patterson Air Force Base, OH 45433 USA

Keywords: Alpha/beta titanium alloys, recrystallization, spheroidization, foil rolling, low-temperature superplasticity, texture

Abstract

Advances in the fundamental understanding of microstructure evolution and plastic flow during primary and secondary processing of titanium alloys are summarized. Examples focus on the recrystallization of the beta phase and spheroidization of alpha lamellae during the breakdown of α/β titanium alloys, challenges in the rolling of foil of α/β and gamma-TiAl alloys, and the effect of microstructure and composition on the superlastic flow behavior of α/β titanium alloys. Particular attention is given to models describing the refinement (or coarsening) of microstructural scale and non-uniformities that may impact forming response during operations such as rolling of sheet and superplastic forming. Current understanding of the persistence of microstructural anomalies such as microtextured regions (aka macrozones) is also described. Finally, recent developments in the characterization of such features via microscopy and ultrasonics are discussed.

Introduction

Conventional ingot-metallurgy (wrought) techniques comprise the most common methods for synthesizing and fabricating titanium-alloy components for the aerospace and other industries [1, 2]. Based on the melting and solidification of large ingots followed by a number of thermomechanical processing (TMP) steps, such approaches provide well-controlled microstructures, minimal defects, and attractive mechanical properties. The various hot-working and heat-treatment steps required to achieve optimal performance are typically performed by primary-metal producers, part vendors, and original equipment manufacturers (OEMs).

Operations performed by primary metal producers usually comprise the melting and re-melting of ingots (via vacuum-arc or cold-hearth techniques) and the conversion of such materials to billets, slabs, sheet etc. via upsetting, drawing/cogging, and rolling to produce semi-finished products such as billets, plate, and sheet. For α/β titanium alloys, wrought processing consisting of β hot working (i.e., working above the $\alpha+\beta \rightarrow \beta$, or β transus, temperature), primary α/β hot working, and β recrystallization is used to breakdown/recrystallize the as-cast, coarse-columnar β grain structure in the starting ingot. Subsequent, *secondary* α/β hot working to produce billet or slab products is applied to spheroidize the lamellar α formed during cooling following the final β recrystallization step. Slabs so produced can then be rolled to plate or sheet at temperatures moderately high in the α/β phase field. Alternatively, plate products are sometimes β annealed again, water quenched to develop a martensitic-α microstructure, and *warm* rolled to sheet to breakdown the fine transformation product. By this means, a refined α-particle size, which promotes low-temperature superplasticity, is obtained.

Common processing operations performed by part vendors and OEMs include closed-die forging of axi-symmetric or more-complex-shaped (e.g., rib-web) components, shape extrusion, ring rolling, superplastic forming, diffusion bonding, and final heat treatment.

In the sections below, a number of advances in the understanding of the mechanisms and/or modeling of microstructure evolution during TMP of titanium alloys are described. Most of these topics focus on the processing of α/β (and near-α) alloys and include the following:

- Static recrystallization of the β phase
- Spheroidization of α lamellae
- Rolling of foil
- Low-temperature superplasticity of ultra-fine alloys
- Deformation and transformation texture formation and the retention/detection of microtextured regions

Beta Recrystallization

The recrystallization of the β phase represents a critical step in the conversion of ingots of α/β (and β) titanium alloys to mill products. During deformation in the single-phase β field, flow-curve measurements have generally exhibited an initial strain-hardening stage followed by steady-state flow, or features indicative of dynamic recovery [3]. Hence, recrystallization of the β-grain structure tends to occur *after* deformation during exposure in the β phase field. The driving force for such recrystallization comprises the stored work imparted by β hot working and/or primary α/β hot working.

Early research [4-7] showed that β grains that grow during β annealing following α/β hot working originate from the small amount of this phase present in the as-hot-worked material. However, the exact mechanism and kinetics were not elucidated. Recent work by Pilchak, *et al.* [8], on the other hand, has shed new light on such issues. In particular, it has been demonstrated that the β phase undergoes a process analogous to *metadynamic* recrystallization characterized by the growth of a small population of pre-existing grains with high-angle boundaries into a matrix of β subgrains (Figure 1). Recrystallization results in the elimination of the very strong, principal texture component, which is associated with the β subgrain structure, and its replacement by a substantially-weaker component possessed by the recrystallized grains which consume the original β matrix (Figure 2).

The rate of migration of the recrystallized grains may be estimated using a simple numerical model originally proposed by Humphreys [9]:

$$\frac{dR}{dt} = M\left(\frac{\bar{\gamma}}{\bar{R}} - \frac{\gamma}{R}\right) \qquad (1)$$

Here, the radius, mobility, and boundary energy of the growing grain(s) are denoted as R, M, and γ, and the average radius and boundary energy of the subgrains as $\bar{R}$ and $\bar{\gamma}$, respectively. For large values of R relative $\bar{R}$, the above expression indicates a linear growth rate whose magnitude is equal to the product of the mobility of the high-angle boundaries, the surface energy of the β subgrains, and the inverse size of the β subgrains.

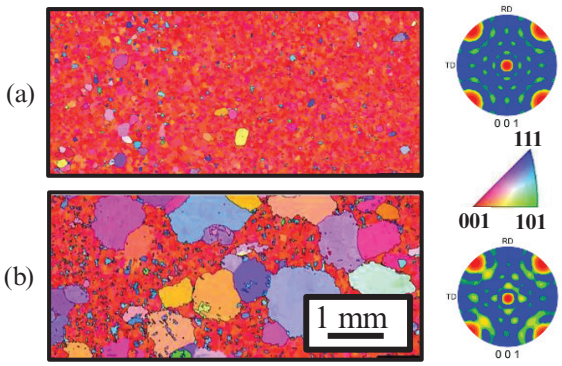

Figure 1. Reconstructed β-phase EBSD normal-direction inverse-pole-figure maps and pole figures for subtransus-hot-rolled Ti-6Al-4V sheet which was β annealed for (a) 31.5 s or (b) 342 s. [8]

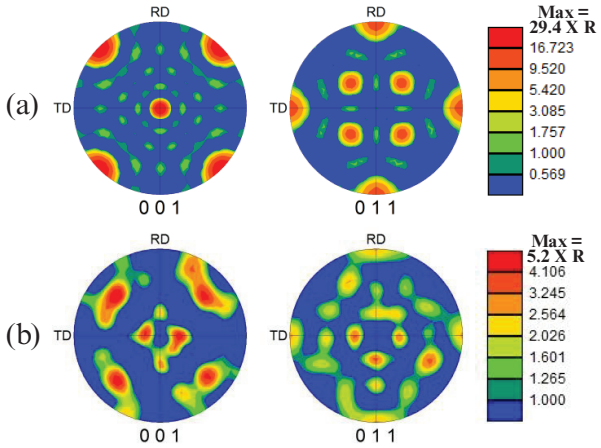

Figure 2. Reconstructed β-phase pole figures for subtransus-hot-rolled Ti-6Al-4V sheet which was β annealed for (a) 31.5 s or (b) 750 s. [8]

Spheroidization of Alpha Lamellae

Spheroidization of a lamellar- or basketweave- α microstructure during TMP of α/β titanium alloys is controlled by several micro-mechanisms. The extent of each depends on the nature of hot working/heat treatment and alloy composition. These factors determine the characteristics of the stored work (which drives spheroidization) and the rate of diffusion.

During deformation, slip processes within the α and β phases and across the α/β interface are key in the development of sub-boundaries within each phase and the loss of coherency of the α/β interface. At low strains (≤ 0.1), slip transmission across low-energy (~50 mJ/m^2), coherent α/β interfaces is possible for the "easy glide" system for which an <a> dislocation in the α phase is nearly parallel to a <111> slip vector in the β phase [10, 11]. By contrast, the activity of the other two <a> slip systems in the α phase gives rise to complex dislocation reactions at α/β interfaces. These dislocation processes decrease coherency and eventually lead to higher-energy (~300 mJ/m^2), incoherent α/β interphase boundaries. The transition from coherent to incoherent typically occurs by a strain of the order of 0.4 to 0.6 [12].

Concurrent with the increase in α/β interphase boundary energy, sub-boundaries form within each phase [13]. Because the equilibrium cell/subgrain size at high temperatures exceeds the thickness of the α and β lamellae/laths in the transformed microstructure, individual sub-boundaries are developed. These sub-boundaries tend to lie normal to the α/β interface and develop misorientations whose magnitude increases approximately linearly with strain [14]. The evolution of the α/β interface energy and the development of sub-boundaries with each phase provide the driving forces for spheroidization.

Alpha-Platelet Fragmentation

During hot working and the early stages of annealing following hot working, a platelet-*fragmentation* process dominates spheroidization behavior. In this case, the sub-boundaries lying normal to the α/β interface are thermodynamically unstable, thus leading to grooves whose full penetration across the thickness of a lamella produces fragmentation (Figure 3a) [15]. The kinetics of grooving can be described using the classical analysis of Mullins [16, 17]. For example, the time for penetration, t_p, is given by the following expression:

$$t_p = \frac{0.2 d_\alpha^3}{Am^3} . \qquad (2)$$

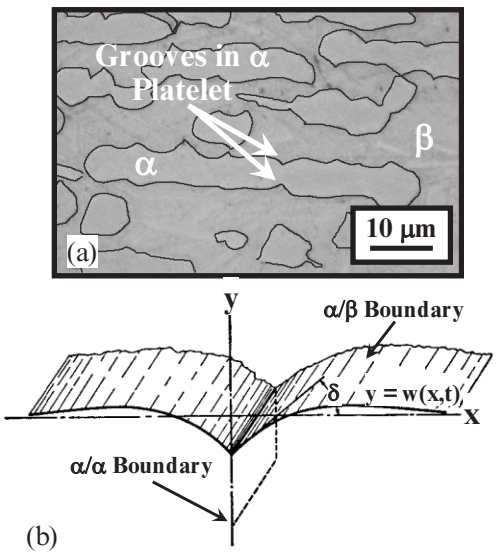

Figure 3. Alpha-platelet fragmentation by the grooving process: (a) Micrograph of Ti-6Al-4V hot worked at 955°C, 0.1 s^{-1} [15] and (b) schematic illustration of the Mullins thermal-grooving mechanism [17].

In Equation (2), d_α denotes the thickness of the α lamella/lath, m_g is the slope of the groove at its symmetry plane (= tan δ, Figure 3b), and A is defined as follows:

$$A = \frac{C_\beta \gamma_{\alpha\beta} \Omega^2 D_\beta}{k_B T} = \frac{C_\beta \gamma_{\alpha\beta} V_M D_\beta}{R_g T}, \qquad (3)$$

In Equation (3), C_β denotes the concentration of the rate-limiting solute in the matrix (expressed in terms of atoms per unit volume or atomic fraction), $\gamma_{\alpha\beta}$ is the α/β interface energy, Ω is the atomic volume, D_β is the diffusivity of the solute through the matrix (β) phase, k_B is Boltzmann's constant, T is the absolute temperature, V_M is the molar volume of the matrix, and R_g is the gas constant. The strong influence of the platelet thickness (d_α) and the slope (m_g) on grooving behavior is demonstrated by the cubic dependence of t_p on these quantities in Equation (2). In turn, the slope m_g is dependent on the energy of the α/β interfaces and α/α sub-boundaries through the surface-tension (force-equilibrium) relation, i.e.,

$$2\gamma_{\alpha\beta} \sin\delta = \gamma_{\alpha\alpha} \qquad (4)$$

Because $\gamma_{\alpha\alpha}$ would tend to be less than or equal to $\gamma_{\alpha\beta}$, the maximum value of δ is ~30°, and thus the slope m_g must be less than or equal to 0.577. The overall dependence of $\gamma_{\alpha\alpha}/\gamma_{\alpha\beta}$ on imposed strain also determines the dependence of fragmentation time on the level of deformation.

Strictly speaking, the expressions for A (Equation (3)) and hence t_p (Equation (2)) are valid only when both the matrix phase and the second phase are terminal solid solutions. For α/β titanium alloys, neither the α nor the β phase is a terminal solid solution. In this case, a composition factor C_F, defined as follows, replaces C_β in Equation (3) [18]:

$$C_F = \frac{(1 - C_\beta)}{(C_\alpha - C_\beta)[1 + \partial \ln r / \partial \ln C_\beta]} \qquad (5)$$

The term in brackets in the denominator of Equation (4) is the thermodynamic factor (for which r ≡ activity coefficient of the solute in the beta phase).

Termination Migration

The complete spheroidization of a lamellar microstructure via boundary grooving/fragmentation during *or* following deformation usually requires strains (and times) much in excess of those that can be imposed in conventional production practices. Moreover, the dislocation substructure which drives boundary grooving tends to be eliminated in relatively short times during *static* heat treatment. At the completion of the pinch-off process, sections of alpha lamellae having a pancake-like shape remain. Subsequent (longer-time) completion of spheroidization thus occurs via termination migration; i.e., the transfer of solute from the periphery to the flat (plan) surfaces of each (assumed non-interacting) alpha lamella, resulting in equiaxed-alpha particles whose diameters are substantially greater than the original platelet thickness [15]. Assuming bulk-diffusion control of the process, the time τ_{vd} to complete spheroidization of a remnant platelet of thickness d_α and diameter w is given by the following relation [19]:

$$\frac{\tau_{vd}}{\tau'} = \frac{\xi^3 - [0.328\xi^{7/3}\left(1+\sqrt{1-0.763\xi^{-4/3}}\right)^2]}{4[\frac{2(1+\xi)}{3(0.5-0.572\xi^{-1/3})} + \frac{0.5\xi^{1/3} + 0.665\xi^{2/3}}{3(0.143+0.934\xi^{-1/3})}]}, \qquad (6a)$$

in which

$$\xi \equiv (w/d_\alpha) + 0.5 \qquad (6b)$$

$$\tau' \equiv d_\alpha^3 R_g T / D_\beta C_F \gamma_{\alpha\beta} V_M . \qquad (6c)$$

The difficulty of spheroidizing remnant-α platelets which are thick is underscored by Equation (6) which reveals a cubic dependence of τ_{vd} on d_α.

Applications

A number of experimental observations have verified the usefulness of the fragmentation and termination-migration/ spheroidization analyses.

As a first example, the applicability of the Mullins analysis for the pinch-off of α platelets has been assessed using the static-heat-treatment observations of Stefansson and Semiatin following hot-working of Ti-6Al-4V [15, 18]. In this work, it was found that boundary splitting was completed in ~14 h at 900°C and ~1 h at 955°C. At both temperatures, the slope m (= tan δ) was measured as ~0.35. Input data at the lower and higher temperatures comprised the values of the composition factor (30.6, 61.3) [20], diffusivity of the rate-limiting solute (vanadium) (0.025, 0.05 $\mu m^2/s$) [21], and the α-platelet thicknesses (~1, 2 μm) [15]. The molar volume (10,440 mm^3) and α/β interphase-boundary energy (0.4 J/m^2) were taken to be the same at both temperatures [20]. Applying Equation (2), the predicted time (1 h) was in excellent agreement with the observation for 955°C, but the prediction for 900°C (32 h) was approximately twice that observed [18]. The difference between measured and predicted times for heat treatment at 900°C was surmised to be due to dislocation substructure in the β matrix retained from prior hot working and a concomitant enhancement in kinetics due to pipe diffusion.

The effect of residual dislocation substructure in the β matrix on solute diffusion and thus grooving kinetics has also been deduced to be important from the work of Zherebtsov, et al. [22]. Among various sets of test conditions, Ti-6Al-4V was *warm* worked and annealed at 800°C. Using material coefficients appropriate for this specific test temperature, including a diffusivity for vanadium in a β matrix *without* residual warm work, the time to complete grooving was predicted to be 190 h. This prediction was considerably greater than that observed, i.e., 20 h, however. Such a difference was explained on the basis of an enhancement of diffusional processes by one order of magnitude for materials with substantial retained substructure from prior working [18, 23].

The validity of Equation (6) to quantify the spheroidization behavior via termination migration and the possible retention of remnant lamellae was established by Semiatin, *et al.* [19] using observations for Ti-6Al-4V heat treated at 955°C. At this temperature, the shapes of the lamellae that existed after the completion of grooving (time ≈ 1 h) approximated the idealized pancake geometry assumed in the diffusion model. As for the grooving mechanism, the diffusion of vanadium through the beta matrix was assumed to be rate-limiting.

Model predictions of τ_{vd}/τ' and hence τ_{vd} for spheroidization of the remnant lamellae are given in Table 1. The predicted values for the spheroidization time for the pancake-shape geometry ranged from approximately 5 to 15 hours for 5 of the 7 platelets; the other two lamellae were predicted to require times of the order of 30 hours. These values of spheroidization time compared well with the measured time of 12-14 h to achieve approximately 90 volume pct. of spheroidized microstructure, as defined by alpha particles with an aspect ratio of less than 2:1 [15, 19]. Thus, the observation of a small volume fraction of modest aspect-ratio, partially-spheroidized lamellae after 14 hours was not surprising.

Table 1. Geometry of Remnant α Lamellae and Model Predictions of Spheroidization Time at 955°C [19]

w (μm)	d_α (μm)	ξ	τ_{vd}/τ'	τ_{vd} (h)
16.4	2.7	6.5	1.39	6.1
17.7	3.2	6.1	1.13	7.8
18.2	3.6	5.5	0.84	8.6
21.8	3.6	6.5	1.39	14.4
24.1	2.3	11.1	6.16	15.6
27.3	3.6	8.0	2.52	26.1
33.2	2.3	15.1	13.6	34.4

Static spheroidization measurements for Ti-6Al-4V at 800°C by Zherebtsov, et al. [22] verified the applicability of Equation (6) at lower temperatures. Assuming that the initial stage of annealing at this temperature had removed all of the warm work in the β matrix, the time to spheroidize remnant lamellae by termination migration was estimated to be 104 h using a diffusivity appropriate for a fully-annealed material. This estimate showed approximate agreement with the measurement (50 h).

The retarding effect of slow-diffusing solutes such as molybdenum on spheoidization of lamellar α by platelet fragmentation and termination migration has also been established. Some key experimental results for Ti-6Al-2Sn-4Zr-2Mo-0.1Si [24] are shown in Figure 4. Here, the dependence of the average aspect ratio of the α lamellae on the level of prestrain and the annealing time at 955°C is summarized. Two regimes are apparent, a short-time period (≤ 2 h), during which the average aspect ratio drops very rapidly, and a longer-time period during

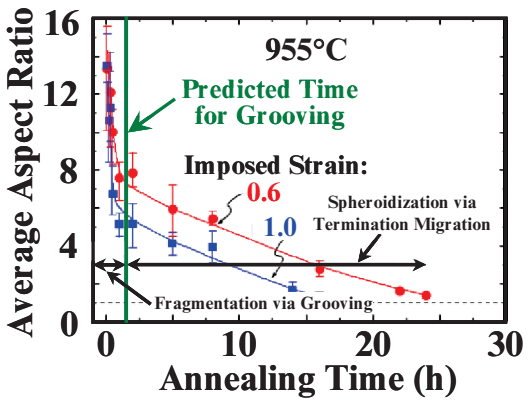

Figure 4. Static-spheroidization behavior of Ti-6Al-2Sn-4Zr-2Mo-0.1Si controlled by platelet fragmentation (short times) and termination migration (long times). [24]

which it decreases more slowly. These two stages are associated with platelet fragmentation via the grooving mechanism and completion of spheroidization via termination migration, respectively [24]. Model predictions of the time required for platelet fragmentation (Equation (2)) and termination migration (using an expression similar to Equation (6) modified for elliptical, rather than round, remnants) incorporating the lower diffusivity of molybdenum (in comparison to vanadium in Ti-6Al-4V) showed good agreement with measurements [24].

An understanding of the kinetics of fragmentation and termination migration and the effects of initial platelet thickness, level of deformation, and TMP temperature on such processes are also critical in establishing methods for developing ultrafine alpha particle sizes possessing low-temperature superplastic-forming capability. Typically, such approaches rely on *warm*-working via rolling or multi-axial forging and low-temperature heat-treatment to breakdown basketweave-alpha microstructures [25-27].

Hot Rolling of Foil

The hot rolling of titanium-alloy sheet products can be quite difficult, especially as the desired final gage becomes thinner. Two examples related to the rolling of foil of gamma (TiAl) titanium-aluminide and α/β titanium alloys illustrate advances and some remaining challenges in this area.

Hot Pack Rolling of Gamma-TiAl Foil

Because of its very limited cold workability, gamma-TiAl must typically be processed via hot-working methods. The production of *sheet* products of these materials is readily accomplished via hot pack rolling [28-31]. In this method, one or more preforms are canned in an expendable, low-cost, ductile alloy (to minimize chilling during rolling), sealed (to provide environmental protection), and rolled conventionally at low to moderate speed. The fabrication of *foil* with a thickness of 0.1 to 0.25 mm by this method is substantially more difficult. The principal challenges comprise (1) the need to control thickness uniformity to avoid final grinding and substantial reductions in product yield and (2) the development of methods to enable easy removal of finished foil(s) from the pack, especially after imparting large strains required to minimize re-canning and thus to achieve cost effectiveness.

A number of special considerations for hot pack rolling of foil of gamma-TiAl-base alloys have been identified [32]. Specifically, a special (proprietary) pack design that enables uniform reduction and ease of de-canning has been found to be very useful. With this design, the thickness is relatively uniform over most of the length of rolled foils (Figure 5a). However, sporadic regions that are locally-thicker have also been observed (Figure 5b). High-magnification SEM backscatter images revealed that the thicker areas contained large un-spheroidized remnants of $\gamma + \alpha_2$ colony microstructure which were surrounded by equiaxed grains of the two phases (Figure 5c). Secondly, electron-backscatter diffraction (EBSD) analysis showed that the {111} plane in the γ phase and the (0001) plane in the α_2 phase of the remnants lay in the rolling plane. These planes are parallel to the habit plane of the $\gamma + \alpha_2$ colony microstructure. The retention of the Burgers orientation relation between the phases suggested that the remnant colonies had undergone very limited, if any, deformation during rolling of both the sheet preform and the final foil product.

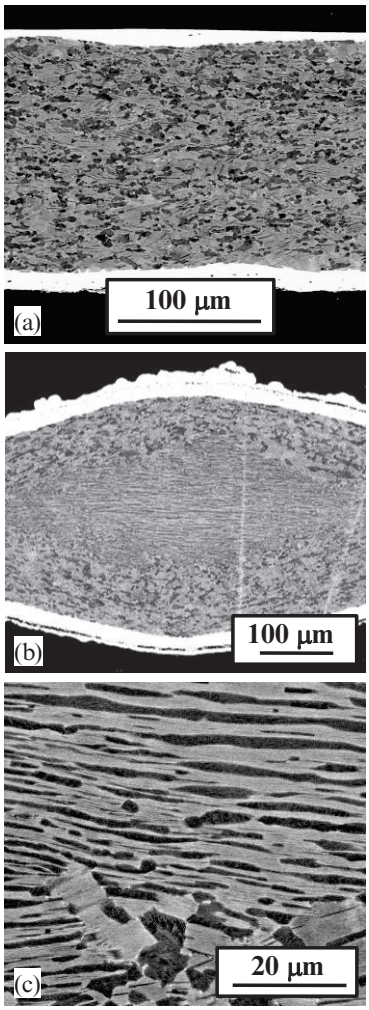

Figure 5. Backscatter-electron images of rolled foil of the $\gamma + \alpha_2$ alloy Ti-45.5Al-2Cr-2Nb (atomic percent): (a) Typical microstructure, (b) region of locally-greater thickness, and (c) higher-magnification micrograph of the central region in (b) showing the presence of a remnant-colony microstructure. In all images, γ is the darker phase and α_2 is the lighter phase. [32]

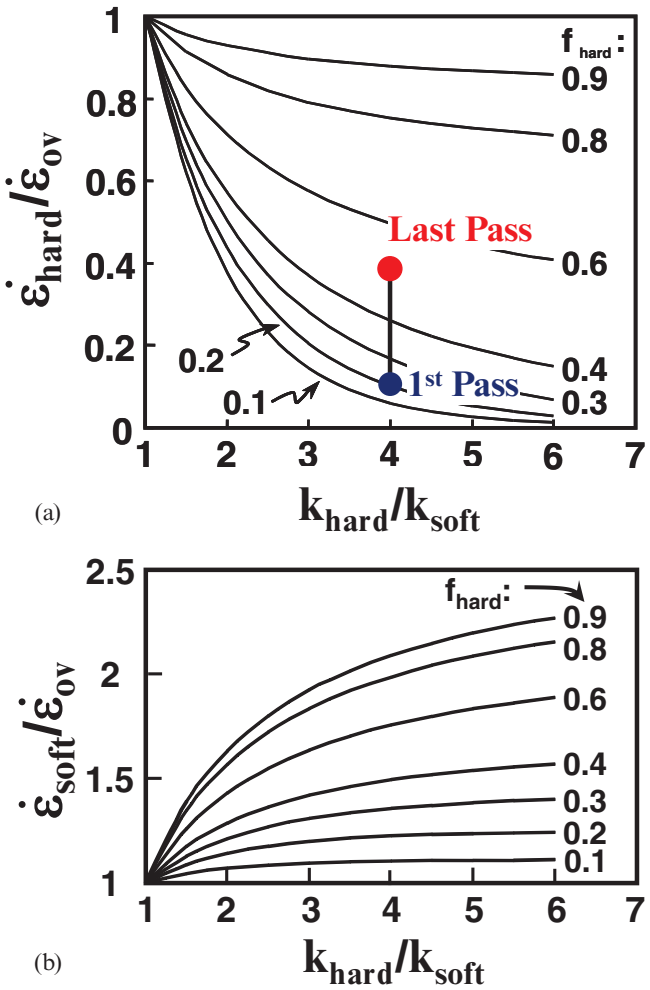

Figure 6. Self-consistent model predictions of the strain rate in the harder and softer phases of a two-phase material as a function of the volume fraction of the hard phase (f_{hard}) and the ratio of the strength coefficients (k) of the two phases.

The relative absence of deformation in remnant colonies can be rationalized based on the flow stress of the colony relative to the surrounding matrix of equiaxed grains and an approximate self-consistent (SC) analysis of the degree of strain-rate partitioning [32]. In particular, the flow stress of the remnant colony was estimated to be approximately *four* times that of the surrounding matrix. The higher flow stress was ascribed to two distinct influences of approximately equal measure: (1) a Hall-Petch-like effect (associated with the small thickness of the lamellae in the colonies) and (2) the hard orientation of the colonies per se. The SC analysis [33] quantified the approximate strain rates (relative to the overall imposed strain rate) in the harder (remnant-colony) and softer (equiaxed-matrix) micro-constituents as a function of the volume fraction of the harder phase (f_{hard}) and the ratio of the strength coeffcients of the phases (k_{hard}/k_{soft}) (Figure 6).

During the first rolling pass, during which the typical remnant colony comprises ~20 pct. of the cross section (i.e., $f_{hard} = 0.2$), the SC analysis indicated that the strain rate in the harder remnant colony would be only one-tenth of the imposed strain rate (Figure 6a). As the overall sample thickness decreases, the remnant colony comprises an increasingly larger fraction of the cross section. Nevertheless, for the case considered in Reference 32, the strain rate in the colony during the last pass was estimated to still be less than one-half of the overall strain rate (Figure 6a).

The efficacy of an initial heat treatment to spheroidize remnant colonies and thus mitigate their deleterious effect on gage control during the pack rolling of gamma-TiAl foil has also been established [32]. For the material used in Reference 32, it was found that almost all of the remnant colonies were eliminated by a heat treatment of 3 h at 1200°C or 0.5 h at 1250°C. Predicted times based on Equation (6), i.e., 1-2 h or 0.25-0.5 h at the lower or higher temperature, respectively, showed reasonable agreement with these observations. By utilizing an initial spheroidization heat treatment, therefore, foil with a maximum thickness variation of ±15 μm has been produced.

Hot Pack Rolling of α/β Titanium Alloy Foil

The rolling of foil of α/β titanium alloys also presents its own distinct challenges. To the present, the greatest success has utilized a series of cold rolling steps in a Sendzimir mill with a number of intermediate anneals to restore cold workability. Such processes tend to be very expensive. An alternate, hot pack-rolling method would thus be very attractive.

Although α/β titanium alloys are very ductile at hot working temperatures, it has been found that a thickness reduction during hot pack rolling to a gage less than ~0.2 mm can sometimes result in a mechanical instability. This instability is manifest by the development of a corrugated-like shape of the foil, consisting of a series of creases in the transverse direction (Figure 7). The spacing of the corrugations is typically of the order of twice the length of the arc of contact.

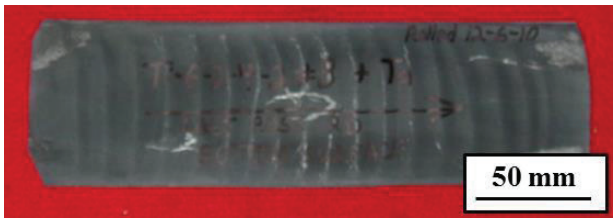

Figure 7. Photograph of a Ti-6Al-2Sn-4Zr-2Mo-0.1Si foil which was hot packed rolled.

A quantitative description of the source of such flow non-uniformity has yet to be developed. There have been a number of investigations of non-uniform flow during the cold rolling of *clad metals* (in which the layers are bonded) [34-37]. Most of these have described the development of diffuse and localized necking in the *harder* component of the laminate as due to a load-instability arising from the generation of rolling-direction secondary tension stresses. Important factors in such failures have been deduced to include the plastic properties and the thickness ratio of the two components. In addition, the diameter of the work rolls has been shown to be important through its impact on redundant shearing in the softer layers of a laminate, thus affecting the relative flow properties of the layers and reducing the propensity for failure of the harder layer [36].

The nature of hot pack rolling of foil of α/β titanium alloys, in which the layers are *not* bonded, appears to be quite different, however. In such cases, a number of factors are likely important. These include the transfer time from the furnace, the rolling speed, the relative thickness of the pack layers, the material comprising the pack covers, and the friction conditions between the preform and covers. The transfer time, rolling speed, cover material, and instantaneous thickness of the pack layers all affect normal-direction temperature gradients which are developed as a result of radiation and conduction (roll chill) heat losses [29]. In concert with the innate flow behaviors of the preform and cover materials, these temperature gradients determine the local flow stress required for deformation and therefore the strain gradient.

Consider the situation in which there is no sliding between the foil preform and the covers. If, for example, the flow stress of the chilled covers is approximately twice that of the hotter preform within the can and the preform thickness is ~10 pct. of the total pack thickness, the results in Figure 6b reveal that the strain rate generated in the preform would be ~50 pct. *greater* than the overall imposed strain rate for the entire pack. Because the material outside the roll gap is non-deforming, there would thus be a *tendency* for the softer preform layer to buckle instead of extending excessively in the rolling direction.

For the actual case in which a low-friction parting agent would be used to enable removal of rolled sheets/foils, relative sliding between the pack components would occur. The magnitude of the sliding would depend on the through thickness pressure, coefficient of friction between the layers, etc. Furthermore, there is the possibility that the neutral point (at which the metal-flow direction changes) for the roll-cover interfaces would lie at a different position than that for the cover-preform interfaces. It may be hypothesized that such a situation could lead to large differences in the flow directions of the pack components that would exacerbate the tendency for corrugation. Research to quantify these phenomena is warranted.

Low-Temperature Superplasticity of Ultra-Fine Ti Alloys

Spurred by the needs of the airframe industry, major progress has been made in the last decade to develop α/β titanium alloys with ultra-fine microstructures that can be processed at lower-than-typical temperatures [38]. Lower processing temperatures enable the use of less-expensive die materials and shorter heating cycles. In addition, the amount of oxygen pickup is reduced, thereby reducing the amount of final machining/pickling and material losses.

Early research in this area was spearheaded in the 1990s by the Institute for Metals Superplasticity Problems (IMSP) in Ufa, Russia under the leadership of Professor G.A. Salishchev. In particular, a low-temperature, multi-axial, isothermal forging technique that yielded billets with an ultra-fine α-particle size (providing low-temperature superplastic flow properties) and the elimination of microtexture was developed [39]; the latter attribute resulted from texture randomization typical of superplastic flow during the final stages of billet processing by this means. Complementary work in the 1990s by Inagaki [25] demonstrated the benefit of a process based on β annealing/water quenching of plate followed by warm rolling to achieve desirable ultra-fine microstructures. Spurred by the seminal research at IMSP, the production of commercial quantities of low-temperature-formable sheet was implemented by VSMPO (Verkhnaya Salda) in Russia in the late 1990s. This was followed by major development efforts throughout the world, focusing first on ultra-fine variants of existing alloys (such as Ti-6Al-4V) and then other material compositions whose scale-up to commercial availability has been achieved during the last 5 years.

Plastic-Flow Behavior

The technological development of ultra-fine α/β Ti alloys suitable for low-temperature superplastic forming has been accompanied by research aimed at quantifying the microstructural basis for the phenomenon. For instance, the effect of α-particle size and shape on flow stress has been established using both uniaxial tension testing of sheet and uniaxial compression of cylindrical samples extracted from billet [40-42]. Typical flow curves from tension tests on two different lots of VSMPO ultra-fine Ti-6Al-4V *sheet* material ("Sheet A" and "Sheet B") are summarized in Figure 8 [41]. In the as-received condition, the microstructure of Sheet A

comprised equiaxed-α particles (~ 2 μm in diameter) in a matrix of β. On the other hand, Sheet B contained elongated-α particles with an average thickness of ~ 3 μm and an aspect ratio of ~2:1 and, to a lesser degree, some equiaxed-α particles. For tests using a constant true strain rate of 10^{-3} s^{-1} (Figure 8a), Sheet A exhibited low initial stresses at 775 and 815°C, followed by flow hardening which was deduced to be related to dynamic coarsening of the α particles. The initial flow stresses for Sheet B were measurably higher at both test temperatures, and large-strain deformation was characterized by flow softening followed by near-steady-state flow (Figure 8a). These latter observations were ascribed to the competition between dynamic spheroidization of the elongated lamellar α (which would lead to smaller α particles and hence flow softening) and dynamic coarsening (which leads to flow hardening as observed for Sheet A). When the imposed strain rate was 10^{-4} s^{-1} (Figure 8b), both lots of sheet exhibited low initial flow stresses and flow hardening. This was as expected for Sheet A. The similarity in behavior of Sheet B was concluded to be a result of dynamic spheroidization at short times/low strains for this rate of deformation.

The flow-stress results from the tension tests of Sheets A and B (and similar measurements from compression tests on samples cut from a Ti-6Al-4V billet with an ultrafine α particle size) were interpreted in the context of a generalized constitutive relation [40, 42, 43], i.e.,

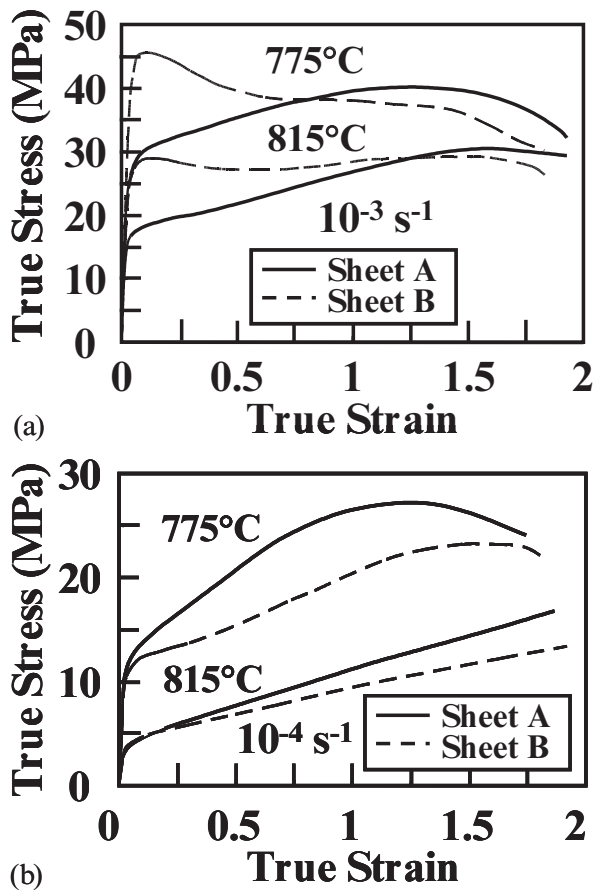

Figure 8: True stress-true strain curves for two different sheets of Ti-6Al-4V with an ultra-fine microstructure tension tested at 775 and 815°C and a constant strain rate of (a) 10^{-3} s^{-1} or (b) 10^{-4} s^{-1}.

$$\dot{\varepsilon} = \left(\frac{ADGb}{k_B T}\right)\left(\frac{\sigma}{G}\right)^n \left(\frac{b}{d}\right)^p \qquad (7)$$

Here, $\dot{\varepsilon}$ is the strain rate, A is a fitting constant, D is a diffusivity pertinent to the dynamic process which limits the rate at which strain concentrations due to grain/interphase-boundary sliding are relaxed in the β matrix, G is the shear modulus of the β phase, b is the length of the Burgers vector in the β phase, k_B is Boltzmann's constant, T is the absolute temperature, σ is the flow stress, n is the stress exponent of the strain rate (=1/m, in which m is the strain-rate sensitivity), d is the α-particle diameter, and p is grain-size exponent of the strain rate. The applicability of Equation (7) for Ti-6Al-4V can be demonstrated by re-arranging it and plotting the calculated values of AD versus 1/T for Sheet A data (at the beginning *and* end of the tension tests) and Sheet B data (only at the end of the tests at which the α particles had become spheroidized) (Fig. 9). In making this graph, the grain size exponent p was taken to be 2 (per Reference 39), and n was assumed to be 1.67 (i.e., m = 0.6). The experimental points from the tension tests were found to lie close to the trend line for the compression results for Ti-6Al-4V *billet* with an ultra-fine microstructure, thus suggesting a unique constitutive behavior irrespective of whether deformation is imposed in tension or compression. Moreover, the apparent activation energy for plastic flow (160 kJ/mol) was found to be essentially identical to that for diffusion of vanadium through the beta matrix in Ti-6Al-4V [44].

Effect of Alloy Composition on Plastic Flow

Commercial production of sheet of ultra-fine Ti-6Al-4V and other α/β titanium alloys in the US has seen major advances during the last five years. For instance, Ti-54M, an alloy originally developed by Timet for its excellent combination of strength, machinability, and ballistic performance [45], has been processed to fine-grain sheet using a method similar to that of Inagaki [25] so that it can be applied for low-temperature forming applications [46]. Early reports in the literature for such sheet material with an initial α-particle size of ~2 to 7 μm revealed strain-hardening response followed by nearly-steady state flow (for strains of ~0.2 or greater); the flow stress was of the order of 15-30 MPa for test conditions consisting of a true strain rate equal to 5 x 10^{-4} s^{-1} and temperature of 775°C [47, 48]. Very recent plastic-flow measurements at the same temperature but a strain rate of 3 x 10^{-4} s^{-1} for Ti-54M sheets with an starting α-particle size of ~2 μm

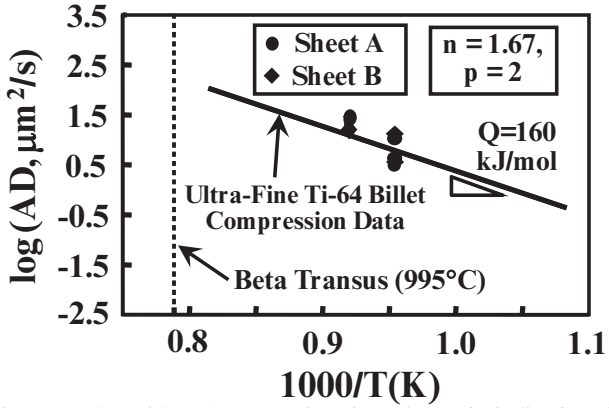

Figure 9. Plot of log (AD) as a function of 1000/T indicating the applicability of a generalized constitutive equation to interpret the plastic-flow response of Ti-6Al-4V.

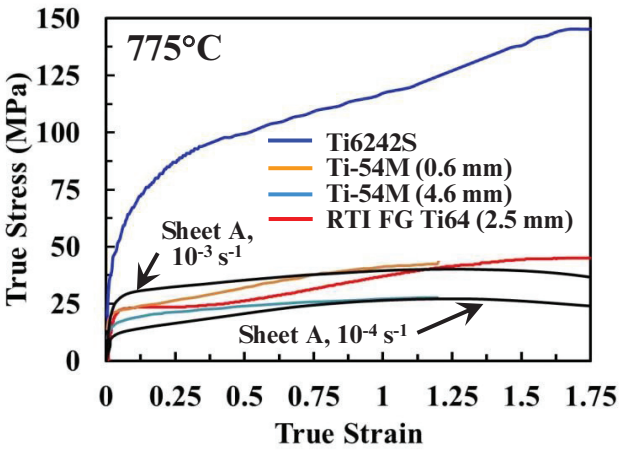

Figure 10. Comparison of the flow response at 775°C/3 x 10^{-4} s^{-1} of ultra-fine α/β titanium alloys consisting of Timet Ti-54M sheet (with two-different thicknesses) [49], RTI fine-grain Ti-6Al-4V [50], and Ti-6Al-2Sn-4Zr-2Mo-0.1Si [51]. The results are compared to the Ti-6Al-4V "Sheet A" flow curves for tests at 775°C and strain rates of 10^{-4} and 10^{-3} s^{-1}, which have been cross plotted from Figure 8.

(4.6-mm-gage material) or ~5 μm (0.6-mm-gage material) were similar to each other, comprising an initial flow stress of 15-20 MPa followed by flow hardening, presumably due to dynamic coarsening [49] (Figure 10).

Flow-curve measurements at 775°C, 3 x 10^{-4} s^{-1} for 2.5-mm thick, fine-grain Ti-6Al-4V sheet produced by RTI International Metals [50] were essentially identical to those for the two gages of Ti-54M sheet tested under the same conditions (Figure 10). The RTI material had a reported starting grain/α-particle size of ~1.5 μm. Not surprisingly, each of the measurements for the Timet and RTI sheet materials in Figure 10 were bracketed by the VSMPO "Sheet A" data measured at 775°C and strain rates of 10^{-4} and 10^{-3} s^{-1} (cross-plotted from Figure 8). The similarity of the results, despite the range of reported α-particle/grain sizes (1.5 to 5 μm), seems to underscore the challenge of measuring this very important microstructural parameter, not only in terms of its mean value, but also its distribution.

The results in Figure 10 are also compared to an approximate flow curve at 775°C/3 x 10^{-4} s^{-1} for Ti-6Al-2Sn-4Zr-2M0-0.1Si. (Using the reported strain-rate and temperature sensitivities of the flow stress, this curve was derived from measurements in Reference 51 for material with an α-particle size of 2.2 μm tested at 750°C and 10^{-4} s^{-1}.) The Ti-6Al-2Sn-4Zr-2Mo-0.1Si flow curve was higher than those for Ti-6Al-4V and Ti-54M by approximately a factor of three, and also exhibited a measurable degree of flow hardening. Assuming similar values for the all of the parameters in Equation (7) for the different alloys, except the diffusivity D, a three-fold higher flow stress would suggest a value of D for Ti-6Al-2Sn-4Zr-2Mo-0.1Si which is approximately one-sixth ($1/3^n = 1/3^{1.67}$) that of the other alloys. This ratio is almost identical to that found in Reference 52. Furthermore, similar to the observations for ultra-fine Ti-6Al-4V and Ti-54M [40-42], the flow hardening noted for Ti-6Al-2Sn-4Zr-2Mo-0.1Si (Figure 10) has been shown to be due to dynamic coarsening [51].

Diffusion Bonding and Friction-Stir Welding

As for a variety of metallic materials, the plastic deformation associated with the flattening of surface asperities plays a key role in the diffusion bonding of α/β titanium alloys. Thus, the low flow stress of these alloys in the ultra-fine-microstructure condition is also beneficial with regard to diffusion bonding at lower-than-normal temperatures. This benefit was first illustrated in the work of Sanders, *et al.* [53] for Ti-6Al-4V, Ti-54M, and ATI 425, both when each alloy was bonded to itself as well as to one of the other alloys in the group. More recently, the bonding of Ti-54M, Ti-6Al-4V, and Ti-6Al-2Sn-4Zr-2Mo-0.1Si with initial α-particle sizes of 2.4, 5.9, and 4.1 μm, respectively, has been investigated [54]. Mirroring the flow-stress trends, bonding of a given alloy to itself could be accomplished at low temperatures/low pressures most readily for Ti-54M and least readily for Ti-6Al-2Sn-4Zr-2Mo-0.1Si. For a given processing temperature and pressure, the bonding of Ti-6Al-2Sn-4Zr-2Mo-0.1Si to either of the other two alloys was better than to itself, thus illustrating the important influence of the deformation resistance of the alloy with lower flow stress during the joining of dissimilar materials.

An increasing demand for larger and more complex titanium sheet-metal parts has also focused attention on the fabrication of *tailor-welded* blanks and their subsequent forming response. In this regard, Sanders and his colleagues have established the effect of process variables during friction-stir welding (FSW) on the microstructures developed within and outside the weld nugget for various α/β titanium alloys and their effect on strain uniformity during forming, e.g., Reference 55. For mill-annealed fine-grain Ti-6Al-4V sheet, for example, the FSW parameters that gave the most uniform flow during subsequent high-temperature tension testing comprised a pin RPM of 325, feed rate of 1.67 mm/s, and forging load (through the thickness) of 55 kN. It was also determined that the removal of tools marks left by the rotating FSW pin (via grinding) was necessary to obtain optimal superplastic forming response after joining.

Texture and Microtexture Formation in α/β Ti Alloys

The formation of crystallographic texture often has a strong effect on both first-tier (e.g., yield strength, modulus) and second-tier (e.g., fatigue, creep) properties, especially for α/β titanium alloys. Some of the recent advances in the quantification of the formation of deformation and transformation textures and the detection and retention of microtexture are briefly summarized in this section.

Deformation Texture

A large amount of research has been conducted to understand the development of *deformation* textures due to processes such as sheet rolling, extrusion, and forging. For the workhorse titanium alloy, Ti-6Al-4V, for instance, deformation mode and processing temperature have a strong influence on texture [56, 57]. In addition, substantial research has been performed to simulate the development of deformation texture in single- and two-phase titanium alloys [58]. This work has utilized various approaches, including the Taylor (isostrain) [59], viscoplastic self- consistent [60], and crystal-plasticity FEM (CPFEM) methods [61].

Recently, the modeling of deformation textures during forging of α/β titanium alloys has focused on a CPFEM technique using the

commercially-available, metal-forming code DEFORM™ [62]. The enhanced FEM software package enables the input of measured starting textures (from x-ray pole figures or EBSD), a routine to partition strain between the α and β phases, a crystal-plasticity module to simulate crystal rotations associated with slip, and a module with several different variant-selection criteria that enables the prediction of the texture of the secondary-alpha platelets that form within the beta-matrix phase during cooling following α/β hot working or heat treatment. With this code, texture predictions for a Ti-6Al-4V pancake forging, which showed approximate agreement with observations, were obtained [62, 63].

Transformation Texture

Textures formed in α/β titanium alloys that result from decomposition of the metastable, high-temperature β phase depend on whether cooling occurs from the two-phase or single-phase field. A number of mechanisms have been observed and reported for each case. However, the TMP conditions that favor each are not well understood.

The observed mechanisms can be partitioned into variant selection at prior β grain boundaries and variant selection *within* prior β grains. For the former instance, it has been reported that the preferred variant has: (1) the minimum possible angle between the habit plane and the grain-boundary plane [64, 65], (2) the close-packed $\boldsymbol{a_1}$ direction lying in the grain-boundary plane, (3) adjacent prior β grains with nearly parallel {110} planes [66, 67], (4) the minimum deviation of grain boundary α from the Burgers orientation relationship with respect to the non-Burgers-related grain [68]. Another important consideration following nucleation is whether or not the grain boundary plane is coincident with a fast-growth direction in the α phase ([0001] and $< 11\bar{2}0 >$). If this condition is satisfied, a particular variant could more quickly cover large areas of grain boundary.

For the case of variant selection during cooling from the two-phase field, all of the above mechanisms may also be operative, but the presence of primary α adds an additional consideration. Specifically, it has been hypothesized that local stresses developed as a result of differences in coefficients of thermal expansion between the α and β phases tend to favor the formation of α variants whose orientation is similar to that of the primary α [5, 69]. Such biasing of the texture of the secondary α by that of the primary α has been modeled based on a minimum strain-energy hypothesis [69]. In other work, it has been postulated that the anisotropic contraction of primary α during cooling may activate slip on selected {110} slip planes in the β phase, thus biasing the secondary-α variants that are formed [70].

Within β grain interiors, it has been hypothesized that $(0001)_\alpha$ will prefer {110} planes that accumulated significant amounts of strain during prior deformation [71]. However, as suggested recently [67], such a rule may not apply when the imposed strain is relatively small (i.e., order of 0.1). Moreover, sympathetic nucleation from the broad faces of existing α laths/colonies has also been reported. This mechanism is based on minimizing the elastic strain energy of the system [72].

While all of these mechanisms are possible, additional research is required to determine the ranges of TMP parameters for which each mechanism may dominate. Suitable models must include a method to predict the orientation of the grain-boundary α and whether this orientation will grow into the β grain as a sideplate or if it will stimulate nucleation of a *different* α variant that grows into the interior. Moreover, it must predict the number of variants formed per grain as a function of cooling rate and the relative fraction of each variant that is formed.

Retention and Characterization of Microtexture Regions

Microtextured regions (MTRs, or macrozones) of nearly common crystallographic orientation often persist following large-strain deformation of near-α and α/β titanium alloys in the two-phase field [63]. The dimensions of these features are typically 100's of microns to several millimeters and have important implications with respect to TMP response, ultrasonic inspection, and fatigue behavior. A number of efforts have been made to characterize MTRs using EBSD data and elastic waves [e.g., 73-77].

EBSD methods can be broadly classified into "real-space" and "Fourier-space" approaches. In the former, similar to classical segmentation protocols, crystallographic misorientation or c-axis mismatch (or both) are calculated between a given pixel and its local neighborhood of pixels. Because two adjacent primary-α particles that are part of the same MTR may not be physically touching in an EBSD data set (due to the potential for secondary-α of a different orientation between them), it is necessary to consider a local window around a given pixel when defining the MTR. Such double-segmentation protocols based on first defining α particles based on misorientation followed by grouping non-interconnected particles into MTRs based on c-axis misorientation have been implemented in the software package DREAM.3D [78]. Pair-correlation functions represent another important way to characterize spatial correlations of similarly-oriented α particles. In this method, vectors of all possible lengths and orientations are sampled within the microstructure to determine the probability that both the head and tail lie within a region of similar orientation. This method is powerful because it incorporates all of the classical statistical measures of microstructure (volume fraction, feature-size distribution, morphology, crystallography) plus the spatial correlation. There is a drawback, however, in that this information is not easily accessible from the correlation function without assuming an underlying distribution of the features; usually Poisson statistics are assumed. Because discrete measurements of features are not made, large features occurring at low frequencies (which may control fatigue behavior) are not easy to capture by this means. On the other hand, the real-space method offers the advantage of providing the upper tail of the distribution to which extreme-value statistics can be applied. The Fourier domain methods are extremely useful when comparing to the results of ultrasonic inversion models, however, because these techniques use the same correlation function as a description of the microstructure [77].

Several important advances have also been made with regard to quantitative measurements of MTRs using ultrasonic (UT) methods. In particular, closed-form solutions for ultrasonic wave propagation and scattering applicable to near-α (and likely α/β) alloys have been obtained [79, 80]. The methods utilize ratios of attenuation and backscattering coefficients collected in various wave-propagation directions for the inversion of experimentally-measured ultrasound data to spatially resolve MTR size. These techniques have been compared with EBSD methods, and

reasonable agreement has been found for mean MTR sizes, thus justifying the UT method for quality control or screening of billet products. These techniques are not sufficiently mature to identify the largest, life-limiting features at this time, however.

Summary and Future Challenges

The evolution of microstructure in α/β (and to a greater or lesser extent in near-α and β-rich) titanium alloys during TMP is controlled by a plethora of phenomena including (1) recovery and recrystallization, (2) boundary grooving/platelet fragmentation, (3) spheroidization via termination migration, and (4) coarsening of α lamellae/particles. An understanding of the kinetics of each mechanism is critical to the design of wrought processes to achieve a desirable level of microstructural uniformity and to avoid defects such as micro-textured regions (MTRs). The understanding and control of microstructure and associated plastic-flow properties is also critical with regard to secondary-forming processes such as foil rolling, superplastic sheet forming, etc. A number of key challenges, ripe for future research, remain, however. These include the following:

- Methods to control/avoid abnormal grain growth during processing in the β phase field, be it during ingot breakdown or final annealing of fracture-critical components.
- Development of an understanding of the evolution of lamellar-α thickness (following β processing) and its effect on subsequent α/β processing of production-scale mill products.
- Methods to predict/minimize/eliminate MTR retention as a function of production ingot/billet conversion practices. Modeling and simulation techniques to predict the size, shape, and population of MTRs.
- Development of simulation techniques that provide *quantitative* location-specific predictions of α-phase deformation textures in complex-shaped forgings.
- Development of *quantitative* rules for α-variant selection during the decomposition of metastable β during cooling from the α/β or β phase field.
- Production-scalable methods to refine/modify the microstructure of hard-to-work alloys to enable low-temperature superplastic forming.

Acknowledgements: Numerous colleagues of the authors have made very significant contributions to the efforts described herein. We gratefully acknowledge the opportunities we have had to work with and benefit from the insights, experience, and, most importantly, friendship of these individuals. These people include J.E. Allison, D.L. Ballard, D. Banerjee, T.R. Bieler, T.F. Broderick, E. Crist, H.L. Fraser, D.U. Furrer, M.G. Glavicic, R.L. Goetz, O.M. Ivasishin, Y. Kosaka, C.S. Lee, P.E. Markovsky, P.L. Martin, S. Mironov, C. H. Park, S.I. Roklin, A.A. Salem, G.A. Salishchev, D.G. Sanders, G.A. Sargent, V. Seetharaman, S.V. Shevchenko, N. Stefansson, V. Venkatesh, J.C. Williams, R.E.A. Williams, A. Woodfield, O. Yu, and S. Zherebtsov.

References

1. G. Luetjering and J.C. Williams, *Titanium* (Berlin: Springer Verlag, 2007).
2. S.L. Semiatin, V. Seetharaman, and I. Weiss, "Hot Working of Titanium Alloys - An Overview," *Advances in the Science and Technology of Titanium Alloy Processing*, ed. I Weiss, *et al.* (Warrendale, PA: TMS, 1997), 3-73.
3. I. Weiss and S.L. Semiatin, "Thermomechanical Processing of Beta Titanium Alloys – An Overview," *Mater. Sci. Eng. A*, A243 (1998), 46-65.
4. H. Moustahfid, N. Gey, M. Humbert, and M.J. Philippe, "Study of the β–α Phase Transformations of a Ti-64 Sheet Induced from a High-Temperature β State and a High-Temperature α+β State," *Metall. Mater. Trans. A*, 28A (1997), 51-61.
5. S.V. Divinski, V.N. Dnieprenko, and O.M. Ivasishin, "Effect of Phase Transformation on Texture Formation in Ti-Base Alloys," *Mater. Sci. Eng. A*, A243 (1998), 201-205.
6. D. Bhattacharyya, G.B. Viswanathan, S.C. Vogel, D.J. Williams, V. Venkatesh, and H.L. Fraser, "A Study of the Mechanism of α to β Phase Transformation by Tracking Texture Evolution with Temperature in Ti–6Al–4V using Neutron Diffraction," *Acta Mater.*, 54 (2006), 231-236.
7. G.C. Obasi, R.J. Moat, D.G.L. Prakash, W. Kockelmann, J. Quinta da Fonseca, and M. Preuss, "In-Situ Neutron-Diffraction Study of Texture Evolution and Variant Selection during the α→β→α Phase Transformation in Ti–6Al–4V," *Acta Mater.*, 60 (2012), 7169-7182.
8. A.L. Pilchak, G.A. Sargent, and S.L. Semiatin, "Early Stages of Microstructure and Texture Evolution during Beta Annealing of Ti-6Al-4V," submitted to *Acta Mater.*, 2015.
9. F.J. Humphreys, "A Unified Theory of Recovery, Recrystallization, and Grain Growth, Based on the Stability and Growth of Cellular Microstructures – I. The Basic Model," *Acta Mater.*, 45 (1997), 4231-4240.
10. A.A. Salem and S.L. Semiatin, "Anisotropy of the Hot Plastic Deformation of Ti-6Al-4V Single-Colony Samples," *Mater. Sci. Eng. A*, A508 (2009), 114-120.
11. S. Suri, G.B. Viswasnathan, T. Neeraj, D.-H. Hou, and M.J. Mills, "Room Temperature Deformation and Mechanisms of Slip Transmission in Oriented Single-Colony Crystals of an α/β Titanium Alloy," *Acta Mater.*, 47 (1999), 1019-1034.
12. S. Zherebtsov, G.A. Salishchev, and S.L. Semiatin, "Loss of Coherency of the Alpha/Beta Interface Boundary in Titanium Alloys during Deformation," *Phil. Mag. Ltrs.*, 90 (2010), 903-914.
13. H. Margolin and P. Cohen, "Evolution of the Equiaxed Morphology of Phases in Ti-6Al-4V", *Titanium '80: Science and Technology*, ed. H. Kimura and O. Izumi (Warrendale, PA: TMS, 1980), 1555-1561.
14. A. Belyakov, W. Gao, H. Miura, and T. Sakai, "Strain-Induced Grain Evolution in Polycrystalline Copper during Warm Deformation," *Metall. Mater. Trans. A*, 29A (1998), 2957-2965.
15. N. Stefansson and S.L. Semiatin, "Mechanisms of Globularization of Ti-6Al-4V during Static Heat Treatment," *Metall. Mater. Trans. A*, 34A (2003), 691-698.
16. W.W. Mullins, "Theory of Thermal Grooving," *J. Appl. Phys.*, 28 (1957), 333-339.
17. W.W. Mullins, "Grain-Boundary Grooving by Volume Diffusion," *Trans. TMS-AIME*, 218 (1960), 354-361.
18. S.L. Semiatin and D.U. Furrer, "Modeling of Microstructure Evolution during the Thermomechanical Processing of Titanium Alloys," *ASM Handbook, Volume 22A: Fundamentals of Modeling for Metals Processing*, Tenth Edition, ed. D.U. Furrer and S.L. Semiatin (Materials Park, OH: ASM International, 2009), 522-535.
19. S.L. Semiatin, N. Stefansson, and R.D. Doherty, "Prediction of the Kinetics of Static Globularization of Ti-6Al-4V," *Metall. Mater. Trans. A*, 36A (2005), 1372-1376.

20. S.L. Semiatin, B.C. Kirby, and G.A. Salishchev, "Coarsening Behavior of an Alpha-Beta Titanium Alloy," *Metall. Mater. Trans. A*, 35A (2004), 2809-2819.
21. S.L. Semiatin, T.M. Brown, T.A. Goff, P.N. Fagin, D.R. Barker, R.E. Turner, J.M. Murry, J.D. Miller, and F. Zhang, "Diffusion Coefficients for Modeling the Heat Treatment of Ti-6Al-4V," *Metall. Mater. Trans. A*, 35A (2004), 3015-3018.
22. S. Zherebtsov, M. Murzinova, G.A. Salishchev, and S.L. Semiatin, "Spheroidization of the Lamellar Microstructure in Ti-6Al-4V Alloy during Warm Deformation and Annealing," *Acta Mater.*, 2011 (59), 4138-4150.
23. I. Weiss and J.J. Jonas, "Interaction between Recrystallization and Precipitation during the High-Temperature Deformation of HSLA Steels," *Metall. Trans. A*, 1979 (10A), 831-840.
24. C.H. Park, J.W. Won, J-W. Park, S.L. Semiatin, and C.S. Lee, "Mechanisms and Kinetics of Static Spheroidization of Hot Worked Ti-6Al-2Sn-4Zr-2Mo-0.1Si with a Lamellar Microstructure," *Metall. Mater. Trans. A*, 43A (2012), 977-985.
25. H. Inagaki, "Enhanced Superplasticity in High Strength Ti Alloys", *Z fur Metallkunde*, 86 (1995), 643-650.
26. S.V. Zherebtsov, G.A. Salishchev, R.M. Galeyev, O.R. Valiakhmetov, S. Yu. Mironov, and S.L. Semiatin, "Production of Submicrocrystalline Structure in Large-Scale Ti-6Al-4V Billet by Warm Severe Deformation Processing," *Scripta Mater.*, 51 (2004), 1147-1151.
27. G.A. Salishchev, E.A. Kudrjavtsev, S.V. Zherebtsov, and S.L. Semiatin, "Low Temperature Superplasticity of Ti-6Al-4V Processed by Warm Multidirectional Forging," *Materials Science Forum*, 735 (2013), 253-257.
28. S.L. Semiatin, D.C. Vollmer, S. El-Soudani, and C. Su, "Understanding the Failure of Near Gamma Titanium Aluminides During Rolling," *Scripta Metall. Mater.*, 24 (1990), 1409-1413.
29. S.L. Semiatin, M. Ohls, and W.R. Kerr, "Temperature Transients During Hot Pack Rolling of High Temperature Alloys," *Scripta Metall. et Mater.*, 25 (1991), 1851-1856.
30. S.L. Semiatin, S.M. El-Soudani, D.C. Vollmer, and C.R. Thompson, "Thermomechanical Processing of Ingot Metallurgy Near Gamma Titanium Aluminides to Refine Grain Size and Optimize Mechanical Properties," US Patent 5,442,847, August 1995.
31. S.L. Semiatin and V. Seetharaman, "Deformation and Microstructure Development During Hot Pack Rolling of a Near-Gamma Titanium Aluminide Alloy," *Metall. Mater. Trans. A*, 26A (1995), 371-381.
32. S.L. Semiatin, B.W. Shanahan, and F. Meisenkothen, "Hot Rolling of Gamma Titanium Aluminide Foil," *Acta Mater.*, 58 (2010), 4446-4457.
33. S.L. Semiatin, F. Montheillet, G. Shen, and J.J. Jonas, "Self-Consistent Modeling of the Flow Behavior of Wrought Alpha/Beta Titanium Alloys under Isothermal and Nonisothermal Hot-Working Conditions," *Metall. Mater. Trans. A*, 33A (2002), 2719-2727.
34. S.L. Semiatin and H.R. Piehler, "Formability of Sandwich Sheet Materials in Plane Strain Compression and Rolling," *Metall. Trans. A*, 10A (1979), 97-107.
35. J-M. Lee, B-R. Lee, and S-B. Kang, "Control of Layer Continuity in Metallic Multilayers Produced by Deformation Synthesis Method," *Mater. Sci. Eng. A*, A406 (2005), 95-101.
36. F. Nowicke Jr, A. Zavaliangos, and H.C. Rogers, "The Effect of Roll and Clad Sheet Geometry on the Necking Instability during Rolling of Clad Metals," *Inter. J. Mech. Sci.*, 48 (2006), 868-877.
37. R. Hebert, G. Marathe, and J. Suri, "Synthesis of Bulk Nanolaminate Materials with Accumulative Roll Bonding," *Proceedings TMS 2009- Volume 1: Materials Processing and Properties* (Warrendale, PA: TMS, 2009), 455-462.
38. P. Comley: "Manufacturing Advantages of Superplastically Formed Fine-Grain Ti-6Al-4V," *J. Mater. Eng. Perf.*, 13 (2004), 660-664.
39. G.A. Salishchev, S. Yu. Mironov, and S.V. Zherebtsov, "Mechanisms of Submicrocrystalline Structure Formation in Titanium and Two-Phase Titanium Alloy during Warm Severe Processing," *Rev. Adv. Mater. Sci.*, 11 (2006), 152-158.
40. G.A. Sargent, A.P. Zane, P.N. Fagin, A.K. Ghosh, and S.L. Semiatin, "Low-Temperature Coarsening and Plastic Flow of an Alpha/Beta Titanium Billet Material with an Ultrafine Microstructure," *Metall. Mater. Trans. A*, 39A (2008), 2949-2964.
41. S.L. Semiatin, P.N. Fagin, J.F. Betten, A. Zane, A.K. Ghosh, and G.A. Sargent, "Plastic Flow and Microstructure Evolution during Low-Temperature Superplasticity of Ultrafine Ti-6Al-4V Sheet Material," *Metall. Mater. Trans. A*, 41A (2010), 499-512.
42. S.L. Semiatin and G.A. Sargent, "Constitutive Modeling of Low-Temperature Superplastic Flow of Ultrafine Ti-6Al-4V Sheet Material," *Key Engineering Materials*, 433 (2010), 235-240.
43. J.E. Bird, A.K. Mukherjee, and J. E. Dorn, "Correlations between High-Temperature Creep Behavior and Structure," *Quantitative Relation between Microstructure and Properties*, ed. D.G. Brandon and A. Rosen (Jerusalem, Israel: Israel Universities Press, 1969), 255-342.
44. S.L. Semiatin, T.M. Brown, T.A. Goff, P.N. Fagin, D.R. Barker, R.E. Turner, J.M. Murry, J.D. Miller, and F. Zhang, "Diffusion Coefficients for Modeling the Heat Treatment of Ti-6Al-4V," *Metall. Mater. Trans. A*, 35A (2004), 3015-3018.
45. Y. Kosaka, S.P. Fox, and J.C. Fanning, "Alpha-Beta Ti-Al-V-Mo-Fe Alloy," US Patent 6,786, 985, September 7, 2004.
46. Y. Kosaka and P. Gudipati, "Method for the Manufacture of Alpha-Beta Ti-Al-V-Mo-V Sheets," US Patent 8,551,264, October 8, 2013.
47. Y. Kosaka and P. Gudipati, "Superplastic Forming Properties of Timetal®54M (Ti-5Al-4V-0.6Mo-0.4Fe) Sheets," *Key Engineering Materials*, 433 (2010), 311-317.
48. Y. Kosaka and P. Gudapati, "Superplastic Properties of Fine Grain Timetal®54M (Ti-5Al-4V-0.75Mo-0.5Fe)," *Ti-2011: Proc. 12th World Conf on Titanium*, ed. L. Zhou, H. Chang, Y. Lu, and D. Xu (Beijing: The Nonferrous Metals Society of China, 2012), 1821-1825.
49. Y. Kosaka and P. Gudipati, "Superplasticity and Characterization of Timetal®54M Sheets," *Proc. Inter. Conf. on Superplasticity in Adv. Mat. (ICSAM) 2015* (Tokyo, Japan), in press.
50. R. Porter and E. Crist, "Ti-6Al-4V Production-Scale Sheet for Low-Temperature SPF Applications," Presentation at AeroMat 2012, Charlotte, NC, June 2012.
51. C.H. Park, B. Lee, S.L. Semiatin, and C.S. Lee, "Low-Temperature Superplasticity and Coarsening Behavior of Ti-

6Al-2Sn-4Zr-2Mo-0.1Si," *Mat. Sci. Eng. A*, A527 (2010), 5203-5211.
52. S.L. Semiatin, T.M. Lehner, J.D. Miller, R.D. Doherty, and D.U. Furrer, "Alpha/Beta Heat Treatment of a Titanium Alloy with a Nonuniform Microstructure," *Metall. Mater. Trans. A*, 38A (2007), 910-921.
53. D. Sanders, L. Hefti, A. Bryant, S. Zeng, H. Guo, P. Gai, and Z. Li, "Diffusion Bonding Performance Test Results for New Titanium Alloys (BAOTI and VSMPO Fine-Grain Ti-6Al-4V, Timetal®54M, and ATI 425) Using Different Temperatures," *Proceedings Inter'l Titanium Association Meeting*, 2010. http://c.ymcdn.com/sites/www.titanium.org/resource/resmgr/2010_2014_papers/SandersDaniel_2010_Manufactu.pdf
54. P. Gudipati and Y. Kosaka, "Diffusion Bonding of Similar and Dissimilar Titanium Alloys," *Ti-2015: Proc. 13th World Conf on Titanium*, ed. V. Venkatesh, *et al.* (Warrendale, PA: TMS, 2015), this volume.
55. D.G. Sanders, M. Ramulu, P.D. Edwards, and A. Cantrell, "Effects on the Surface Texture, Superplastic Forming, and Fatigue Performance of Ti-6Al-4V Friction Stir Welds," *J. Mat. Eng. Perf.*, 19 (2010), 503-509.
56. M. Peters and G. Luetjering, "Control of Microstructure and Texture in Ti-6Al-4V," *Titanium '80: Science and Technology*, ed. H. Kimura and O. Izumi (Warrendale, PA: TMS, 1980), 925-935.
57. J.C. Williams and E.A. Starke, Jr., "The Role of Thermomechanical Processing in Tailoring the Properties of Aluminum and Titanium Alloys," *Deformation, Processing, and Structure*, ed. G. Krauss (Materials Park, OH: ASM International, 1984), 279-354.
58. S.L. Semiatin, M.G. Glavicic, S.V. Shevchenko, O.M. Ivasishin, Y.B. Chun, and S.K. Hwang, "Modeling and Simulation of Texture Evolution during the Thermomechanical Processing of Titanium Alloys," *ASM Handbook, Volume 22A: Fundamentals of Modeling for Metals Processing*, Tenth Edition, ed. D.U. Furrer and S.L. Semiatin (Materials Park, OH: ASM International, 2009), 536-552.
59. M.G. Glavicic, R.L. Goetz, D.R. Barker, G. Shen, D. Furrer, A. Woodfield, and S.L. Semiatin, "Modeling of Texture Evolution during Hot Forging of Alpha/Beta Titanium Alloys," *Metall. Mater. Trans. A*, 39A (2008), 887-896.
60. D. Dunst and H. Mecking, "Analysis of Experimental and Theoretical Rolling Textures of Two-Phase Titanium Alloys," *Zeitschrift für Metallkunde*, 87 (1996), 498-507.
61. N.R. Barton and P.R. Dawson, "On the Spatial Arrangement of Lattice Orientation in Hot-Rolled Multiphase Titanium," *Model. Simul. Mat. Sci. Eng.*, 9 (2001), 433-463.
62. M.G. Glavicic, *et al.*, "Progress in the Advanced Titanium Microstructure and Modeling Program," *Ti-2015: Proc. 13th World Conf on Titanium*, ed. V. Venkatesh, *et al.* (Warrendale, PA: TMS, 2015), this volume.
63. M.G. Glavicic and V. Venkatesh, "ICME of Titanium: Current Capabilities Being Developed under the Metals Affordability Initiative," *JOM*, 66, No. 7 (2014), 1310-1320.
64. J.K. Lee and H. Aaronson, "Influence of Faceting upon the Equilibrium Shape of Nuclei at Grain Boundaries – Two Dimensions," *Acta Metall.*, 23 (1975), 799-808.
65. J.K. Lee and H. Aaronson, "Influence of Faceting upon the Equilibrium Shape of Nuclei at Grain Boundaries – Three Dimensions," *Acta Metall.*, 23 (1975), 809-820.
66. D. Bhattacharyya, G.B. Viswanathan, R. Denkenberger, D. Furrer, and H.L. Fraser, "The Role of Crystallographic and Geometrical Relationships between α and β Phases in an α/β Titanium Alloy," *Acta Mater.*, 51 (2003), 4679-4691.
67. S.L. Semiatin, K.T. Kinsel, A.L. Pilchak, and G.A. Sargent, "Effect of Process Variables on Transformation-Texture Development in Ti-6Al-4V Sheet Following Beta Heat Treatment," *Metall. Mater. Trans. A*, 44A (2013), 3852-3865.
68. R. Shi, V. Dixit, H.L. Fraser, Y. Wang, "Variant Selection of Grain-Boundary α by Special Prior β Grain Boundaries in Titanium Alloys," *Acta Mater.*, 75 (2014), 156-166.
69. M. Humbert, L. Germaine, N. Gey, P. Bocher, and M. Jahazi, "Study of the Variant Selection in Sharp Textured Regions of Bimodal IMI 834 Billet," *Mat. Sci. Eng. A*, A430 (2006), 157-164.
70. L. Zeng and T.R. Bieler, "Effects of Working, Heat Treatment, and Aging on Microstructural Evolution and Crystallographic Texture of α, α′, α″, and β phases in Ti–6Al-4V Wire," *Mat. Sci. Eng. A*, A392 (2005), 403-414.
71. N. Gey, M. Humbert, M.J. Philippe, and Y. Combres, "Modeling the Transformation Texture of Ti-64 Sheets after Rolling in the β-Field," *Mat. Sci. Eng. A*, A230 (1997), 68-74.
72. C. Shen, J.P. Simmons, and Y. Wang, "Effect of Elastic Interaction on Nucleation: I. Calculation of the Strain Energy of Nucleus Formation in an Elastically Anisotropic Crystal of Arbitrary Microstructure," *Acta Mater.*, 54 (2006), 5617-5630.
73. A.L. Pilchak, C.J. Szczepanski, J.A. Shaffer, A.A. Salem, and S.L. Semiatin, "Characterization of Microstructure, Texture, and Microtexture in Near-Alpha Titanium Mill Products," *Metall. Mater. Trans. A*, 44A (2013), 4881-4890.
74. A. A. Salem, J.B. Shaffer, D.P. Satko, S. L. Semiatin, and S. R. Kalidindi, "Workflows for Integrating Mesoscale Heterogeneities in Material Structure with Process Simulation of Titanium Alloys," *Integrating Materials and Manufacturing Innovation*, 3, no. 24 (2014).
75. M. Humbert, A. Moreau, E. Uta, N. Gey, P. Bocher, and C. Bescond, "Analysis of Backscattered Ultrasound Amplitude of Ti-5.8Al-4Sn-3.5Zr-0.7Nb-0.5Mo-0.3Si Samples in Terms of their Microstructures and Local Textures ," *Acta Mater.*, 2009 (57), 708-714.
76. A. Bhattacharjee, A.L. Pilchak, O. Lobkis, J.W. Foltz, S.I. Roklin, and J.C. Williams, "Correlating Ultrasonic Attenuation with Microtexture in a Near-Alpha Titanium Alloy," *Metall. Mater. Trans. A*, 42A (2011), 2358-2372.
77. A.L. Pilchak, J. Li, S.I. Rokhlin, "Quantitative Comparison of Microtexture in Near-Alpha Titanium Measured by Ultrasonic Scattering and Electron Backscatter Diffraction," *Metall. Mater. Trans. A*, 45A (2014), 4679-4697.
78. M.A. Groeber and M.A. Jackson, "DREAM.3D: A Digital Representation Environment for the Analysis of Microstructure in 3D," *Integrating Materials and Manufacturing Innovation*, 3, no. 5 (2014).
79. O.I. Lobkis and S.I. Rokhlin, "Characterization of Polycrystals with Elongated Duplex Microstructure by Inversion of Ultrasonic Backscattering Data," *Appl. Phys. Lett.*, 96 (2010), article 161905, 1–3.
80. L. Yang, J. Li, O.I. Lobkis, and S.I. Rokhlin, "Ultrasonic Propagation and Scattering in Duplex Microstructures with Application to Titanium Alloys," *J. Nondestruct. Eval.*, 31 (2012), 270–283.